

Journal of Materials Chemistry A

Accepted Manuscript



This is an *Accepted Manuscript*, which has been through the Royal Society of Chemistry peer review process and has been accepted for publication.

Accepted Manuscripts are published online shortly after acceptance, before technical editing, formatting and proof reading. Using this free service, authors can make their results available to the community, in citable form, before we publish the edited article. We will replace this *Accepted Manuscript* with the edited and formatted *Advance Article* as soon as it is available.

You can find more information about *Accepted Manuscripts* in the [Information for Authors](#).

Please note that technical editing may introduce minor changes to the text and/or graphics, which may alter content. The journal's standard [Terms & Conditions](#) and the [Ethical guidelines](#) still apply. In no event shall the Royal Society of Chemistry be held responsible for any errors or omissions in this *Accepted Manuscript* or any consequences arising from the use of any information it contains.



Selective and irreversible adsorption of mercury(II) from aqueous solution by a flower-like titanate nanomaterial†

Wen Liu,^{a,b} Xiao Zhao,^b Ting Wang,^a Jie Fu,^{*c} Jinren Ni,^{*a}

Received 00th Jun 2015,
Accepted 00th Jun 2015

DOI: 10.1039/x0xx00000x

www.rsc.org/

A novel flower-like titanate nanomaterial (titanate nanoflowers, TNFs) was synthesized through hydrothermal method using nano-anatase and sodium hydroxide, and used for mercury(II) removal from aqueous solution. The large surface area (187.32 m² g⁻¹) and low point of zero charge (3.04) of TNFs facilitated the adsorption of cations. Adsorption experiments indicated that TNFs could quickly capture 98.2% of Hg(II) from solution within 60 min at pH 5. The maximum adsorption capacity of Hg(II) was as large as 454.55 mg g⁻¹ calculated by the Langmuir isotherm model. Moreover, selective adsorption of Hg(II) by TNFs was observed with the coexistence of other conventional cations (i.e., Na⁺, K⁺, Mg²⁺ and Ca²⁺) even at 10 times concentration of Hg(II). XRD analysis indicated that the prepared TNFs was a kind of tri-titanate composed of edge-sharing triple [TiO₆] octahedron and interlayered Na⁺/H⁺, and ion-exchange between Hg²⁺ and Na⁺ was the primary adsorption mechanism. Furthermore, it was interesting that the basic crystal structure of TNFs, tri-titanate (Ti₃O₇²⁻), transformed into hexa-titanate (Ti₆O₁₃²⁻) after adsorption, resulting in the trap of Hg(II) into the lattice tunnel of this hexa-titanate. Desorption experiments also confirmed the irreversible adsorption due to Hg(II) trapped in TNFs, which achieved safe disposal of this highly toxic metal in practical application.

Introduction

Titanate nanomaterials have drawn great attentions in recent years due to their special physicochemical properties, like large surface area and pore volume, good stability, ion-exchange property, photo-electricity function and quantum size effect.¹⁻³ Hydrothermal treatment is widely used to fabricate such materials,² and various titanate nanomaterials with different morphologies, including titanate nanotubes (TNTs), titanate nanofibers, titanate nanowires, titanate nanosheets, etc., are synthesized under different hydrothermal conditions.⁴⁻⁸ The ion-exchange property of the titanate nanomaterials is greatly concerned in the environmental remediation area, which leads to the efficient capture of metal ions (especially toxic heavy metal cations).⁹ Many studies are focused on adsorption behaviours and mechanisms of a variety of metal cations by titanate nanomaterials, like adsorption of common heavy metal cations (Pb²⁺, Cd²⁺, Cr³⁺, Cu²⁺ and Ni²⁺),¹⁰⁻¹³ radioactive cations

(Sr²⁺, Ba²⁺, Cs⁺ and Th⁴⁺),¹⁴⁻¹⁶ metal and metalloid anions (Cr(VI) and As(V))¹⁷⁻²⁰.

Mercury (Hg) is a highly toxic and bio-accumulative contaminant. In waters, Hg always exists as a number of complex chemical and biological species and is involved in various transformation processes, of which Hg methylation has been the most concerned environmental problem.²¹ Methylmercury (MeHg) is a potent neurotoxin, which can accumulate through the aquatic food chain and show great threats to ecosystem and human health.²¹ Therefore, removal of Hg ions from aqueous solution or blocking the transfer of Hg ion into waters has always been a very serious issue, and lots of techniques are developed for remediation of Hg contaminated waters. Compared to the methods like chemical precipitation,²² bioprocess technology,²³ electrochemical coagulation,²⁴ and membrane process,²⁵ adsorption is more efficient, easier to operate, lower cost, and more environment-friendly.^{26, 27} Thus, develop of novel Hg adsorbents, especially high efficient nano-adsorbents, has been an important issue in this area. Considering the excellent adsorptive performance of titanate nanomaterials, removal of Hg from aqueous solution using these materials is available. Although many studies reported the adsorption of common heavy metals by titanate nanomaterials, there is little information on adsorption of Hg, and both the behaviours and mechanisms are largely unknown. In addition, the conventional Na⁺, K⁺, Ca²⁺ and Mg²⁺ usually coexist in the heavy-metal (e.g. Hg) contaminated waters, which with high concentrations may greatly affect the adsorption of target heavy metal ions on materials.^{10, 28, 29}

^a The Key Laboratory of Water and Sediment Sciences, Ministry of Education, Department of Environmental Engineering, Peking University, Beijing 100871, China

^b Environmental Engineering Program, Department of Civil Engineering, Auburn University, Auburn, AL 36849, USA

^c School of Civil and Environmental Engineering, Georgia Institute of Technology, Atlanta, GA 30332, USA

* Corresponding author, J. Fu, Tel.: +1 334 524 0068, fax: +1 334 524 0068, E-mail: jie.fu@ce.gatech.edu; J.R. Ni, Tel: +86-10-6275-1185, Fax: +86-10-6275-6526, E-mail: nijinren@jee.pku.edu.cn

† Electronic Supplementary Information (ESI) available: Parameters for adsorption kinetic and isotherm models; Adsorption capacity of Hg(II) by typical adsorbents; HSAB hardness and hydration energy of metal ions; Atomic percent of TNFs; BET surface area, size distribution and zeta potential varying as pH of TNFs; And Hg(II) species distribution as pH. See DOI: 10.1039/x0xx00000x

Thus, an adsorbent with high selectivity for Hg(II) adsorption is also important for practical application.

Ion-exchange is demonstrated to be the dominant mechanism for most of metal cations adsorption onto layered sodium titanate.^{9,10,30} Moreover, it is widely accepted that ion-exchange just occurs in the interlayers while the basic titanate skeleton hardly changes due to the stable crystal structure,^{6,10,14,31} resulting in easy desorption and reuse of the materials.³¹ However, adsorption behaviours may be different regarding to the various structures and compositions of titanate materials, and the lattice form may change after adsorption for some of titanate materials with less stable structures. For example, Yang *et al.* found that there was a phase transition from Na₂Ti₃O₇ to Na₂Ti₆O₁₃ after adsorption of ¹³⁷Cs⁺ by titanate nanofibers.¹⁵ Therefore, more studies are needed to further investigate the phase transition in the adsorption process.

In this study, a novel flower-like titanate material (titanate nanoflowers, TNFs) was synthesized through hydrothermal method, and adsorption behaviours of Hg(II) were systematically studied. In addition, selective capture of Hg(II) by TNFs was observed after competitive adsorption experiments. Furthermore, phase deformation of titanate and trap of Hg(II) in the adsorption process were detailedly discussed. The overall objective of this work is to develop a new titanate material for efficiently capture of Hg(II), and clearly interpret the selective and irreversible adsorption mechanisms.

Experimental section

Chemicals

All chemicals were of analytical grade without further purification. The precursor used to synthesize TNFs, TiO₂ (anatase, 99.7%, mean diameter of 25 nm) was purchased from Sigma-Aldrich (St. Louis, MO, USA). NaOH, sodium ethylene diamine tetraacetic acid (EDTA) and absolute ethanol (also used to synthesize TNFs) were obtained from Acros Organics (Fair Lawn, NJ, USA). HgCl₂ (Fisher Scientific, Fair Lawn, NJ, USA) was dissolved in high-purity deionized water (Millipore Co., 18.2 MΩ·cm) to form a stock solution of 1000 mg L⁻¹. In addition, the stock solution of Na⁺, K⁺, Mg²⁺ and Ca²⁺ was prepared using the corresponding chloride salt and DI water, respectively.

Synthesis and characterization of TNFs

TNFs were prepared through a facile hydrothermal method under low NaOH concentration and temperature in this study. First, 1.2 g of anatase was dispersed into an 8 M NaOH solution with a total volume of 66.7 mL. After magnetically stirred for 12 h, the mixture was transferred into a Teflon reactor with stainless steel coating, and then heated at 120 °C for 48 h. After that, the white precipitates were washed with deionized (DI) water to neutral. Finally, TNFs were obtained after dried at 80 °C for 4 h in an oven.

Morphology of TNFs was analysed on a Tecnai30 FEG transmission electron microscopy microscope (TEM, FEI, USA) operating at 300 kV. The crystal phases of TNFs before and after

adsorption were recorded using a Dmax/2400 X-ray diffractometer (XRD, Rigaku, Japan) using Cu Kα radiation (λ = 1.5418 Å) at a scan rate (2θ) of 4°/min. Brunauer-Emmett-Teller (BET) specific surface areas of the materials were determined via nitrogen adsorption-desorption isotherms at -196 °C using an ASAP2010 adsorption apparatus (Micromeritics, USA). Pore volume and mean pore diameter were also measured by means of the nitrogen adsorption volume at a relative pressure of 0.99. Element composition and the oxidation state of samples were recorded on an AXIS-Ultra X-ray photoelectron spectroscopy (XPS, Kratos, England) using Al Kα X-ray source at 15 kV and 15 mA. Standard C 1s peak (Binding energy, E_b = 284.80 eV) was used to eliminate static charge effects. Raman spectra of the materials were recorded on a RM-1000 (Renishaw, UK) with 514 nm excitation from a He-Ne laser. Zeta potentials of samples at different pH were obtained using a Nano-ZS90 Zetasizer (Malvern Instruments, UK).

Adsorption experiments

All the adsorption experiments were carried out in glass erlenmeyer flasks (total volume of 100 mL) with Hg(II) solution and TNFs. For kinetics studies, 0.01 g of TNFs was added into 50 and 100 mg L⁻¹ of Hg(II) solution with a total volume of 50 mL. After pH was adjusted to 5 using dilute HCl and NaOH aqueous solution (aq.), the mixture was shaken (200 rpm, 25±0.5 °C) for 240 min. Samples were taken at set time intervals and then immediately filtrated through a 0.22 μm polyethersulfone (PES) membrane. For adsorption isotherm tests, the initial Hg(II) concentration varied from 20 to 200 mg L⁻¹ with a TNFs dosage of 0.2 g L⁻¹, and the mixture was shaken for 120 min to reach the adsorption equilibrium. For effect of pH on adsorption, initial pH of Hg(II) solution (50 mg L⁻¹) was varied from 2 to 9 by adjusting with HCl and NaOH aq and TNFs dosage was also set as 0.2 g L⁻¹. Experiment on adsorption isotherm of Hg(II) by P25 was also conducted with initial Hg(II) concentration from 2–30 mg L⁻¹ and material dosage of 0.2 g L⁻¹ at pH 5.

Competitive adsorption experiments were conducted as the initial Hg(II) concentration was fixed at 50 mg L⁻¹ while the coexisting inorganic ion (including Na⁺, K⁺, Mg²⁺ and Ca²⁺) concentration varied from 50 to 500 mg L⁻¹. TNFs dosage was set as 0.2 g L⁻¹ and solution pH was adjusted to 5. After 120 min's adsorption, the Hg(II) concentration in the supernate was determined after filtration. Mg²⁺ and Ca²⁺ concentration was also measured after the corresponding experiment, respectively.

Concentrations of Hg(II) and other metal ions were measured on an inductively coupled plasma-optical emission spectrometry (ICP-OES, Prodigy, Leeman, USA). The adsorption capacity (Q_e, mg g⁻¹) of Hg(II) on TNFs and removal efficiency (R, %) at equilibrium are calculated from:

$$Q_e = \frac{(C_0 - C_e)V}{m} \quad (1)$$

and

$$R = \frac{(C_0 - C_e)}{C_0} \times 100\% \quad (2)$$

where C_0 (mg L^{-1}) is the initial Hg(II) concentration, C_e (mg L^{-1}) is the equilibrium Hg(II) concentration, V (mL) is the solution volume, and m (g) is the mass of TNFs.

Desorption and regeneration experiments

After the initial adsorption of 50 mg L^{-1} Hg(II) by 0.2 g L^{-1} TNFs at pH 5, the suspension was centrifuged (10,000 rpm, 5 min) and the supernatant was removed. Afterwards, 50 mL of DI water, HNO_3 (0.1 M, 0.5 M and 1 M), NaOH (0.1 M, 0.5 M and 1 M) and EDTA (0.1 M, 0.5 M and 1 M) solution was added respectively and the mixture was shaken for another 120 min to start the desorption tests. Both the Hg(II) concentration after adsorption (C_e) and desorption (C_d) were determined, and the desorption rate D (%) is calculated by:

$$D = \frac{C_d - C_e}{C_0 - C_e} \times 100\% \quad (3)$$

An acid-base treatment was conducted to evaluate the regeneration efficiency of TNFs. After TNFs with Hg(II) adsorbed were treated with HNO_3 (0.5 and 1 mM), NaOH solution (0.5 and 1 mM) was used to restore the $-\text{ONa}$ sites based on our previous study.³¹ The regenerated TNFs was reused to adsorb Hg(II) as the foregoing conditions.

Results and discussion

Morphology of TNFs

As shown in TEM images (Fig. 1), the precursor, nano-anatase is a kind of spherical nanoparticle with a diameter of 20–30 nm (Fig. 1a). After synthesis of TNFs, peony-like nanoflowers are observed (Fig. 1b). The new materials present as well-developed ray flowers with a diameter of $\sim 0.5 \mu\text{m}$ and are aggregated into flower clusters. In addition, the petals of the TNFs are further confirmed as titanate nanosheets (Fig. 1d). The BET surface area and single point total pore volume of TNFs was determined as $187.32 \text{ m}^2 \text{ g}^{-1}$ and $0.86 \text{ cm}^3 \text{ g}^{-1}$, respectively, which are benefited to the adsorption of metal ions. Moreover, the N_2 adsorption-desorption isotherms on TNFs fitted type IV isotherms with H3 hysteresis loops according to BDDT classification,³² suggesting the presence of mesopores (2–50 nm) in the material (Fig. S1a†). The pore size of TNFs mainly exhibits a bimodal distribution, as shown in Fig. S1b†. Pores with peak diameter at $\sim 30 \text{ nm}$ are assigned to the internal space of curly nanosheets while larger pores with peak diameter at 70–80 nm are attributed to the gaps between the nanosheets and voids in the aggregation of the materials.^{33–35} The point of zero charge (pH_{PZC}) for TNFs was determined as 3.04 (Fig. S2†), and the relatively low pH_{PZC} indicates an outstanding adsorption capacity for metal cations at wide pH ranges.

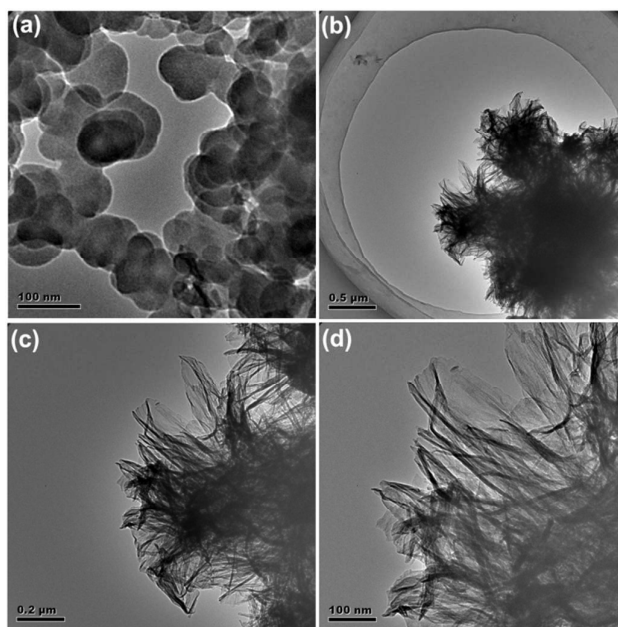


Fig. 1 TEM images of (a) anatase and (b, c and d) TNFs.

Adsorption of Hg(II) by TNFs

Adsorption of Hg(II) onto TNFs over time is displayed in Fig. 2a. It is observed that TNFs could quickly capture of Hg(II) from aqueous solution. The adsorption mainly occurred in the first 10 min and could rapidly reach equilibrium within 60 min either for initial Hg(II) concentration at 50 or 100 mg L^{-1} . The equilibrium adsorption capacity was as high as 245.5 and 407.4 mg g^{-1} , with a removal efficiency of 98.2% and 63.0% for Hg(II) at 50 or 100 mg L^{-1} , respectively. Pseudo-first-order and pseudo-second-order models are used to analyse the kinetics results, which are expressed as:^{36, 37}

$$\text{Pseudo-first-order model: } Q_t = Q_e - Q_e \exp(-k_1 t) \quad (4)$$

$$\text{Pseudo-second-order model: } \frac{t}{Q_t} = \frac{1}{k_2 Q_e^2} + \frac{t}{Q_e} \quad (5)$$

where Q_t and Q_e (mg g^{-1}) are the adsorption capacities of Hg(II) at time t (min) and equilibrium, respectively. k_1 (min^{-1}) and k_2 ($\text{g mg}^{-1} \text{ min}^{-1}$) are the rate constants of the pseudo-first-order and pseudo-second-order kinetic models, respectively.

Table S1† lists the parameters for the two kinetic models. Obviously, the pseudo-second-order model can better describe the adsorption kinetic results ($R^2 = 1$), indicating the rate-controlling step for adsorption was chemical interaction, exhibited by the initial diffusion of Hg^{2+} ions from solution to TNFs' surface, and then interaction between $-\text{ONa}/-\text{OH}$ groups of TNFs and Hg^{2+} ions.³⁷

Adsorption isotherm result is presented in Fig. 2b, which is further analysed using Langmuir³⁸ and the Freundlich³⁹ models, as expressed below:

$$\text{Langmuir model: } Q_e = \frac{Q_{max} b C_e}{1 + b C_e} \quad (6)$$

$$\text{Freundlich model: } Q_e = K_f C_e^{1/n} \quad (7)$$

in which Q_e (mg g^{-1}) and C_e (mg g^{-1}) are the adsorption capacity and concentration of Hg(II) at equilibrium. Q_{max} (mg g^{-1}) represents the maximum adsorption capacity, and b (L mg^{-1}) is the Langmuir constant related to the adsorption energy. K_f ($(\text{mg g}^{-1}) \cdot (\text{L mg}^{-1})^{1/n}$) is the Freundlich constant related to adsorption capacity and n is the heterogeneity factor indicating the adsorption intensity of the adsorbates.

The corresponding parameters for adsorption isotherm models are listed in Table S2†. The isotherm data fit well with the Langmuir model ($R^2 = 0.9997$), with an extremely large maximum adsorption capacity of 454.55 mg g^{-1} . It is suggested that monolayer adsorption occurs on the TNFs, and there was no interaction between adsorbed Hg(II) ions.³⁸ In comparison, the adsorption performance of TNFs for Hg(II) is much better than most of the conventional adsorbents, such as activated carbon (55.6 mg g^{-1}),⁴⁰ multi-walled carbon nanotubes (87.7 mg g^{-1}),⁴¹ mesoporous silica (200.6 mg g^{-1} for SBA-15 and 140.4 mg g^{-1} for MCM-41),⁴² *Aspergillus versicolor* biomass (75.6 mg g^{-1}),⁴³ and even ion-exchange resin (358.7 mg g^{-1})⁴⁴ (Table S3†). In addition, the Hg(II) adsorption capacity on TNFs is much larger than that on P25, which is only 19.4 mg g^{-1} calculated by Langmuir isotherm model (Fig. S3†).

For effect of pH on adsorption (Fig. 2c), at low pH (2 and 3) below pH_{PZC} of TNFs, the Hg(II) adsorption capacity was relatively small (11.4 mg g^{-1} at pH 2 and 113.6 mg g^{-1} at pH 3). It was because TNFs were positively charged in these pH ranges, thus capture of Hg(II) cations was inhibited due to electrostatic repulsion. In addition, abundant of H^+ would compete for adsorption sites with Hg(II) cations at low pH. When pH increased to 4, the adsorption capacity sharply increased to 224.6 mg g^{-1} because of the surface charge of TNFs turned to negative (Fig. S2†), which could efficiently capture Hg(II) cations from solution. At $\text{pH} \geq 5$, increasing negative charges located on TNFs' surface resulted in large adsorption capacities, with an almost complete removal of Hg(II) ($> 98\%$). Moreover, the precipitation of Hg(II) (in the form of $\text{Hg}(\text{OH})_2$) at higher pH (> 6) should also not be ignored (Fig. S4†), and co-precipitation with TNFs would be the dominate adsorption mechanism for these ions.⁴⁵

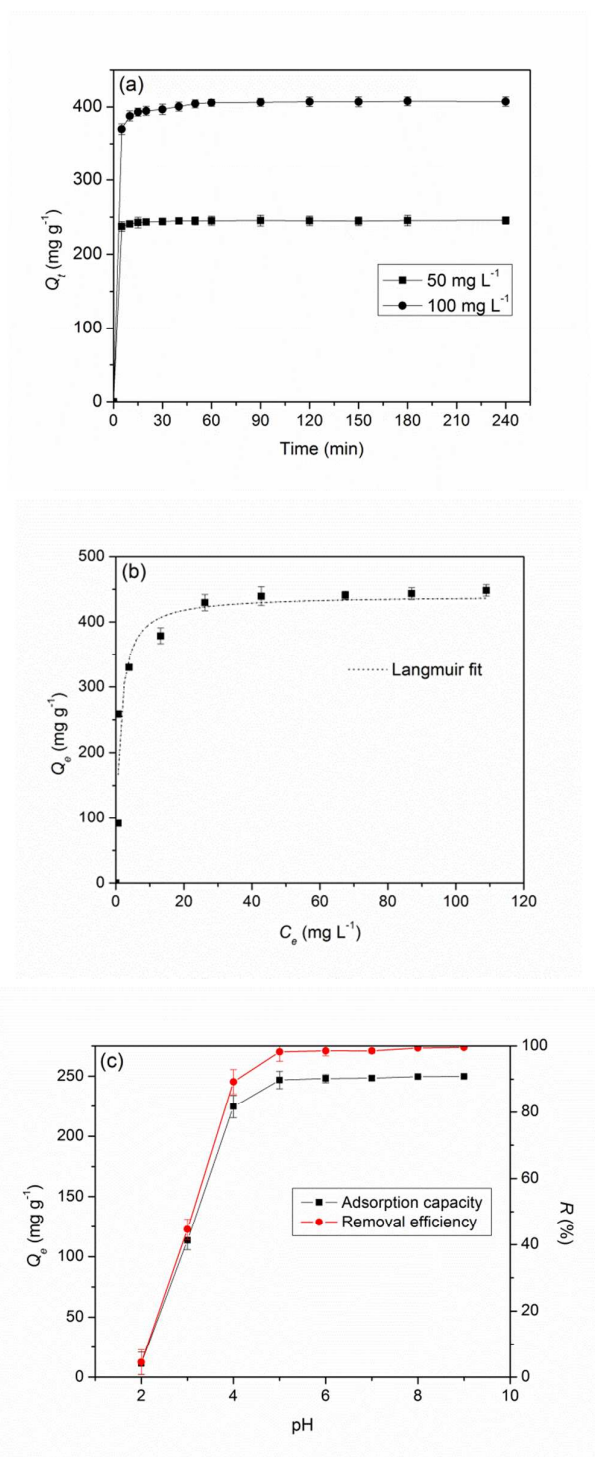


Fig. 2 (a) Adsorption kinetic, (b) isotherm and (c) pH effect on adsorption of Hg(II) by TNFs.

Selective adsorption of Hg(II) in the presence of coexisting inorganic ions

Considering the high concentration of Hg(II) and coexisting inorganic ions (e.g. Na^+ , K^+ , Mg^{2+} and Ca^{2+}), in wastewater from mining, metal smelting, coal purification procedure, and so on,²⁸ the

effect of these conventional inorganic ions on adsorption of Hg(II) are shown in Fig. 3a. It was found that the coexisting Na⁺ and K⁺ just slightly inhibited adsorption of Hg(II) onto TNFs, as the adsorption capacity only decreased by 5.4% and 5.7% even at inorganic ion concentration of 500 mg L⁻¹. The inhibition effects caused by the divalent ions (Mg²⁺ and Ca²⁺) were a little larger than that by monovalent ions. However, large Hg(II) adsorption capacity of 226.5 and 218.9 mg g⁻¹ (decreased by 7.8% and 10.9%) were still obtained in the presence of 500 mg L⁻¹ of Mg²⁺ and Ca²⁺, respectively. A parameter called separation factor (α) is introduced to further evaluate the adsorption preference of TNFs for Hg(II) in the presence of Mg²⁺ and Ca²⁺, which seem to show more obvious inhibition effect on adsorption than Na⁺ and K⁺. The separation factor (α) is defined as:¹⁰

$$\alpha_i^{\text{Hg}} = \frac{Q_{e,\text{Hg}} C_{e,i}}{Q_{e,i} C_{e,\text{Hg}}} \quad (8)$$

where $Q_{e,\text{Hg}}$ and $Q_{e,i}$ are the adsorption capacities of Hg and coexisting metal i at equilibrium (mg g⁻¹), while $C_{e,\text{Hg}}$ and $C_{e,i}$ are the equilibrium concentrations of Hg and metal i (mg L⁻¹). Generally, $\alpha_i^{\text{Hg}} = 1$ implies that the adsorption selectivity of Hg(II) is equivalent to that of coexisting metal i , while when $\alpha_i^{\text{Hg}} > 1$ means Hg(II) is preferred to be adsorbed by TNFs. As shown in Fig. 3b, $\alpha_i^{\text{Hg}} \gg 1$ for each binary system at various Mg²⁺ and Ca²⁺ concentrations ($\alpha_{\text{Mg}}^{\text{Hg}} > 710$ and $\alpha_{\text{Ca}}^{\text{Hg}} > 360$), indicating the obviously selective adsorption of Hg(II) by TNFs. Smaller separation factor is gained at higher Mg²⁺/Ca²⁺ initial concentration, due to the superiority of the metal concentration. In addition, smaller separation factor is observed with Ca²⁺ existing, indicating a larger inhibition effect on Hg(II) adsorption caused by Ca²⁺.

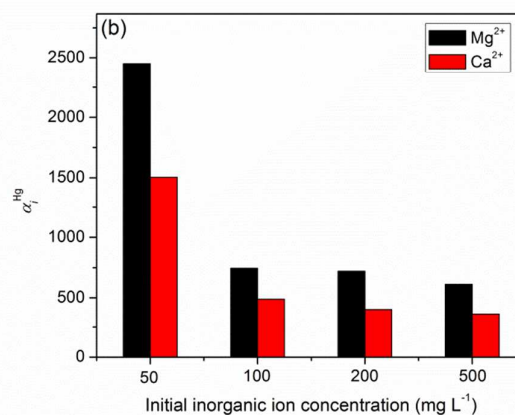
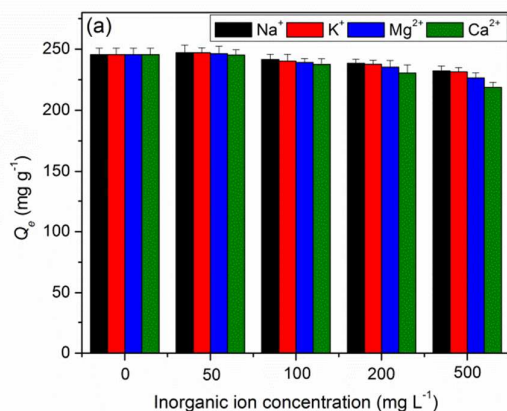


Fig. 3 (a) Effect of coexisting inorganic ions on adsorption of Hg(II) by TNFs, and (b) separation factor for Hg(II) adsorption onto TNFs in the presence of Mg²⁺ and Ca²⁺.

The strong affinity of Hg(II) to TNFs is mainly due to the lower hardness based on Hard-Soft Acid-Base (HSAB) principle.^{6,10} In our previous studies, we proposed the adsorption of metal cations onto sodium titanate materials via three steps: (1) dissociation of hydrated metal ion into bare ion; (2) capture of bare ion by negatively charged titanate via electrostatic attraction; (3) ion-exchange of bare ion with interlayered Na⁺/H⁺.¹⁰ For step 1, metal ion with lower hydration energy can more easily transform into bare ion; For step 2, metal cation with higher valence has larger electrostatic attraction force; For step 3, according to Pearson's HSAB Principal,⁴⁶⁻⁴⁸ hard acids bind strongly to hard bases and soft acids bind strongly to soft bases. TNFs with a composition of sodium titanate can be recognized a "hard acid-soft base" material, while metal cations in solution is considered to be Lewis acid, thus metal cation with lower hardness is more inclined to exchange with the interlayered Na⁺/H⁺ (high hardness). Therefore, although Hg(II) has larger hydration energy than Na⁺, K⁺ and Ca²⁺,⁴⁹ the much lower hardness (7.7) results in relatively stronger affinity to TNFs than the four inorganic ions (Table. S4†).⁶ Furthermore, Hg(II) ion with larger ionic radius and strong affinity to titanate leads to the deformation of titanate structure and irreversible adsorption, which also enhances its competitive adsorption onto TNFs, and it will be detailedly discussed in the next section.

Adsorption mechanism: deformation of TNFs and irreversible adsorption

XRD patterns of nano-anatase, TNFs before and after adsorption of Hg(II) are shown in Fig. 4. After hydrothermal treatment for synthesis of TNFs, all the anatase transformed into titanate. The peaks at $2\theta \approx 10^\circ$, 24° , 28° , 48° and 62° in the spectra of TNFs are assigned to sodium tri-titanate with a universal chemical formula of Na₂Ti₃O₇ (JCPDs No.31-1329).^{9,50} Specifically, the peak at $2\theta \approx 10^\circ$ represents the interlayer distance (d_{200}) of tri-titanate. Typically, tri-titanate is composed of triple [TiO₆] octahedron as the basic skeleton and interlayered Na⁺, which are the ion-exchange sites for cations (Fig. 5). For TNFs with Hg(II) adsorbed (TNFs-Hg), it is

ARTICLE

interesting that the crystal phase of TNFs totally transformed into hexa-titanate ($\text{Na}_2\text{Ti}_6\text{O}_{13}$, JCPDS No. 73-1398),^{50, 51} also accompanying with a decrease of interlayer distance (d_{200}) from 0.837 nm of tri-titanate to 0.575 nm of hexa-titanate. Generally, formation of hexa-titanate needs more energy than that of tri-titanate,^{50, 52} so Hg(II) adsorption onto TNFs is an exothermic reaction, and the accumulation of heat in lattice unit may result in the deformation of titanate crystal phase, as well as great collapse of the interlayers. Previous studies also widely reported the metal cation (e.g. Tl(I), Tl(III) and Cu(II)) adsorption by TNTs was an exothermic reaction.^{12, 45} Furthermore, no crystalline of Hg(II) or relegated compounds formed after adsorption, indicating ion-exchange just processed in the interlayers.

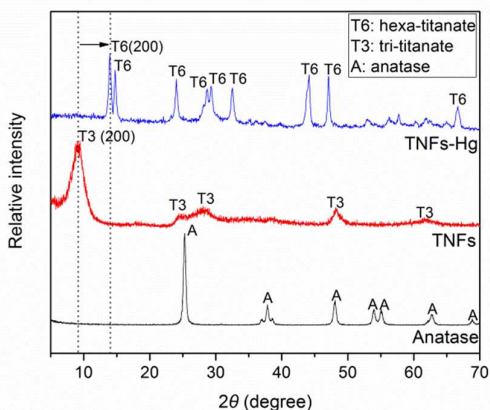
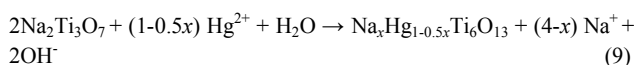


Fig. 4 XRD patterns of anatase and TNFs before and after Hg(II) adsorption.

A schematic diagram depicting the adsorption mechanism of Hg(II) by TNFs is displayed in Fig. 5. Before adsorption, TNFs exhibit in the crystal phase of tri-titanate: triple corrugated ribbons of edge-sharing $[\text{TiO}_6]$ octahedrons compose the basic structure and Na^+ locates in the interlayers. After ion-exchange of Hg^{2+} with Na^+ , the Hg^{2+} will draw the triple $[\text{TiO}_6]$ octahedron unit to corner-shared ones, and as a result, hexa-titanate is formed. In addition, hexa-titanate possesses microporous tunnel structures, which can efficiently entrap the adsorbed Hg^{2+} , thus achieving irreversible adsorption and safe disposal of this highly toxic heavy metal. Assuming that one Hg^{2+} can exchange with two Na^+ , the adsorption and phase deformation process can be simply expressed as:



Journal of Materials Chemistry A

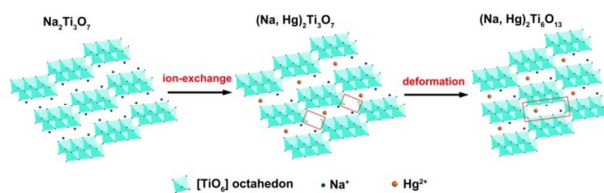


Fig. 5 Schematic diagram of adsorption mechanism of Hg(II) by TNFs.

Similarly, Yang *et al.* also found the phase transition from tri-titanate to hexa-titanate for titanate nanofibers after adsorption of radioactive Cs^+ .¹⁵ However, deformation of titanate was not observed for TNTs (sodium tri-titanate) after adsorption of Cs^+ .¹⁵ Same results were also drawn in our previous studies, for the structure of TNTs before and after adsorption of heavy metal cations (e.g. Pb^{2+} , Cd^{2+} , Cu^{2+} and Cr^{3+}), the triple $[\text{TiO}_6]$ skeleton did not change while only interlayered peak shifted due to ion-exchange.^{10, 30, 53} Therefore, It can be concluded that phase deformation from tri-titanate to hexa-titanate in the adsorption process mostly occur when both of the following two conditions are satisfied: (1) metal cation with large ionic radius which can draw the terminal oxygen atoms in $[\text{TiO}_6]$ unit together; (2) materials with not very stable titanate structure, such as titanate nanofibers and titrate nanosheets (microstructure of TNFs in this study).

Elemental composition of TNFs before and after Hg(II) adsorption was further analysed by XPS (Fig. 6), and the corresponding atomic composition is presented in Table S5†. Before adsorption, the main elements composed TNFs are Na, Ti and O, which is consistent with the crystalline of sodium titanate obtained from XRD. Considering the basic structure of $\text{Na}_2\text{Ti}_3\text{O}_7$ and washing procedure after hydrothermal treatment for synthesis (residual H^+ in the interlayers), the chemical composition of TNFs can be written as $\text{Na}_{1.59}\text{H}_{0.41}\text{Ti}_3\text{O}_7 \cdot 2.4\text{H}_2\text{O}$. Therefore, The theoretical maximum exchange capacity for divalent ion is 3.01 mmol/g. Considering the experimental Hg(II) adsorption capacity of 1.22 mmol/g at initial concentration of 50 mg/L and pH 5, not all the exchangeable ions (Na^+ and H^+) were replaced via adsorption, and Na^+ ion-exchange was primary rather than H^+ . After Hg(II) adsorption, the intensity of Na 1s peak greatly decreased while a new peak assigned to Hg 4f appeared (Fig. 6a), and composition of TNFs transformed to $\text{Na}_{0.34}\text{H}_{0.38}\text{Hg}_{0.64}\text{Ti}_6\text{O}_{13} \cdot 2.6\text{H}_2\text{O}$. This result is in accordance with our previous studies, i.e., adsorption of metal cations is mainly contributed to the ion-exchange with interlayered Na^+ .³⁰ Due to the large hardness of H^+ ($+\infty$), Na^+ plays the dominant role in the ion-exchange process. In the high resolution of O 1s spectra, the peak at ca. 532 and 530 eV presents the O from adsorbed surface hydroxyl groups ($-\text{OH}$) and crystal lattice $[\text{Ti}-\text{O}_6]$.^{54, 55} The fraction of lattice O decreased from 93.2% to 89.9% after Hg(II) adsorption, resulting from combination of terminal O atoms in the $[\text{TiO}_6]$ via adsorption (shown in Fig. 5). There is almost no change for the Ti 2p peaks (Ti 2p_{1/2} and Ti 2p_{3/2}) before and after adsorption, suggesting deformation of $\text{Ti}_3\text{O}_7^{2-}$ to $\text{Ti}_6\text{O}_{13}^{2-}$ does not change the basic lattice unit of $[\text{TiO}_6]$, while just alters the composition form of $[\text{TiO}_6]$. Moreover, after adsorption, all the Hg presents as Hg^{2+} , indicating adsorption mechanism is ion-exchange between Hg^{2+} and interlayered Na^+ .⁵⁶

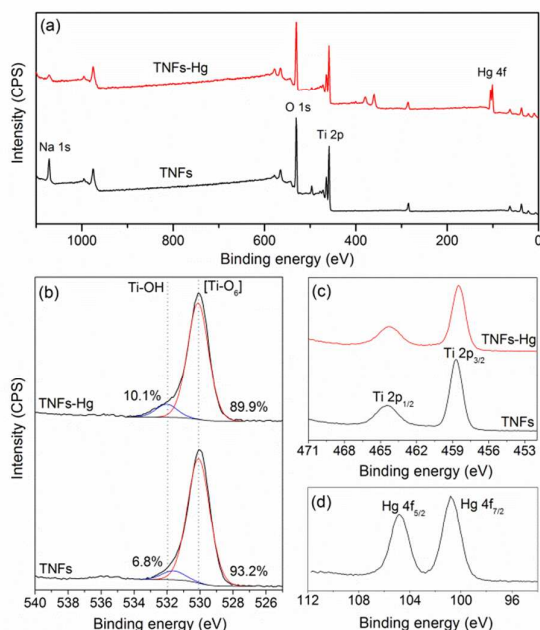


Fig. 6 (a) XPS survey, (b) high resolution of O 1s, (c) Ti 2p and (d) Hg 4f spectra for TNFs before and after adsorption.

As described in Raman spectra (Fig. 7), the spectra of TNFs is similar to that of titanate materials synthesized under low NaOH concentration or low temperature,^{6, 57} which is consistent with the hydrothermal conditions of 8 M NaOH and 120 °C in this study. Specifically, the peak at 909 cm⁻¹ is assigned to the short Ti–O stretching vibration related to Na⁺, namely, Ti–O–Na. After adsorption of Hg(II), a typical hexa-titanate spectra was observed. The peak at 920 cm⁻¹ belongs to the moderate-length Ti–O bond, and moreover, the characteristic peaks for tri-titanate at ca. 309 cm⁻¹ (vibration of the short Ti–O band) and 883 cm⁻¹ (vibration of the short Ti–O band) did not appear. All the findings indicates that there is no terminal oxygen atom in the crystal structure of TNFs after adsorption, and all the oxygen atoms at the surface become linearly coordinated by two titanium atoms, thus titanate with a structure of Na₂Ti₆O₁₂ formed after adsorption.^{15, 58}

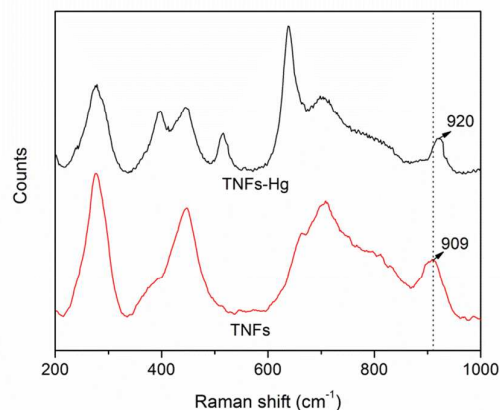


Fig. 7 Raman spectra of TNFs before and after Hg(II) adsorption.

Desorption of Hg(II) from TNFs and material regeneration

Desorption rates of Hg(II) from TNFs via different treatments are presented in Fig. 8. It is found that almost no Hg(II) desorbed from TNFs when H₂O ($D = 0.9\%$), NaOH ($D = 2.4\%$ at 1 M) and EDTA ($D = 7.5\%$ at 1 M) were used as desorbents. Although ion-exchange of Hg²⁺ with Na⁺ was the dominate adsorption mechanism, further addition of Na⁺ (even with high concentration) could not replace the adsorbed Hg(II), indicating adsorption of Hg(II) by TNFs was irreversible. Deformation from tri-titanate to hexa-titanate resulted in efficiently trap of Hg(II) in the tunnels (Fig. 5), which facilitated the safe disposal of Hg(II) after adsorption. Under HNO₃ treatment, the release of Hg(II) into solution was mainly due to destroy of titanate structure and dissolution of titanate (especially at higher HNO₃ concentration at 1 M).^{31, 59, 60} The acid treatment may provide an available method for reuse of TNFs after desorption and regeneration. We developed an acid-base method through initial HNO₃ and subsequent NaOH treatment to evaluate the regeneration efficiency of TNFs. It was found the TNFs could be partially regenerated with treated with 0.5 mM HNO₃ and NaOH (Fig. S5), because the desorption rate was low at low HNO₃ concentration (Fig. 8). In addition, adsorption capacity of Hg(II) on regenerated TNFs could reach up to 207.3 mg g⁻¹ (just decreasing by 15.6% compared to original TNFs), while decreased to 163.4 mg g⁻¹ (by 33.5%) after 3 desorption-regeneration cycles due to damage of structure of TNFs. However, such high acid concentration is virtually nonexistent in real environment, so Hg(II) can hardly be desorbed and pose any threat to environment after practical application, and stable trap of Hg(II) into TNFs is reliable.

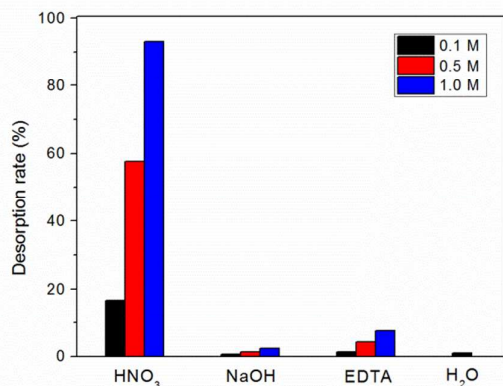


Fig. 8 Desorption rate of Hg(II) from TNFs under different treatment.

Conclusions

Titanate nanoflowers were synthesized through a facile hydrothermal method using nano-anatase and NaOH. Titanate nanosheets composed the peony-like flowers, which possessed a large specific surface area of (187.32 m² g⁻¹) and low point of zero charge (3.04). XRD analysis indicated that TNFs was a kind of sodium tri-titanate, composing of triple [TiO₆] octahedron as the basic skeleton and interlayered H⁺/Na⁺. Adsorption of Hg(II) by TNFs could quickly reach the equilibrium within 60 min and pseudo-second-order model could well describe the kinetic process. The maximum adsorption capacity of Hg(II) onto TNFs could reach up to 454.55 mg g⁻¹ according to the Langmuir isotherm model, which was much larger than that on other conventional adsorbents. More importantly, TNFs could selectively capture Hg(II) in the presence of other inorganic cations, as the adsorption capacity only decreased by 7.8% and 10.9 % even at 10 times concentration of Mg²⁺ and Ca²⁺ to that of Hg(II). Furthermore, there was a phase deformation for TNFs after adsorption of Hg(II), whose tri-titanate (Ti₃O₇²⁻) structure transformed into hexa-titanate (Ti₆O₁₃²⁻), resulting in formation of titanate lattice tunnel and trap of Hg(II). XPS analysis further confirmed the TNFs performed as tri-titanate of Na_{1.59}H_{0.41}Ti₃O₇·2.4H₂O and phase deformation. In addition, desorption of Hg(II) from TNFs by DI water and NaOH solution was hard (< 3%), demonstrating the irreversible adsorption due to trap of Hg(II) in hexa-titanate. This study proposed an efficient method to removal of Hg(II) using a novel titanate nanomaterial, which can achieve the goal of safe disposal of this highly toxic heavy metal.

Acknowledgments

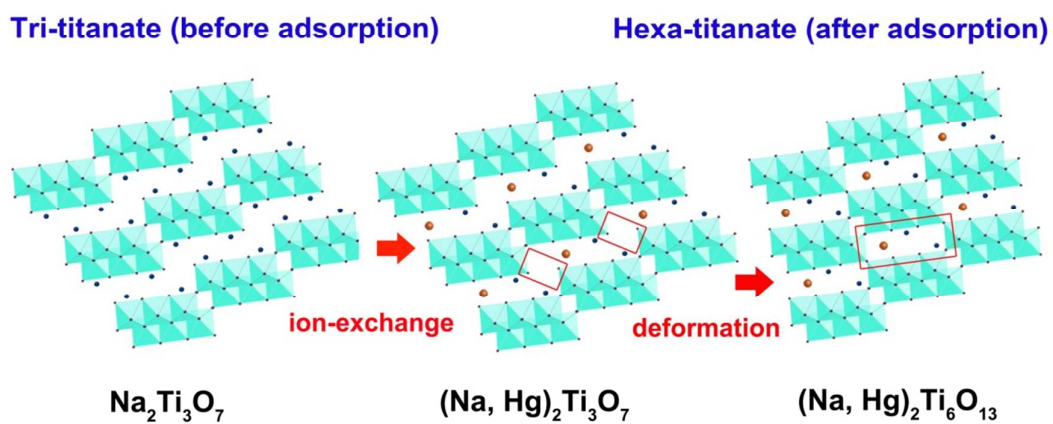
Financial support from National Natural Science Foundation of China (Gran No.51379010) is very much appreciated. Supports from U.S. Department of the Interior Bureau of Ocean Energy Management (M12AC00013) and Collaborative Innovation Center for Regional Environmental Quality of China are also acknowledged.

Notes and references

- D. V. Bavykin, J. M. Friedrich and F. C. Walsh, *Adv. Mater.*, 2006, 18, 2807-2824.
- H.-H. Ou and S.-L. Lo, *Sep. Purif. Technol.*, 2007, 58, 179-191.
- A. Thorne, A. Kruth, D. Tunstall, J. T. S. Irvine and W. Z. Zhou, *J. Phys. Chem. B*, 2005, 109, 5439-5444.
- Z. Y. Yuan and B. L. Su, *Colloids Surf. A*, 2004, 241, 173-183.
- Q. Chen, W. Z. Zhou, G. H. Du and L. M. Peng, *Adv. Mater.*, 2002, 14, 1208-1211.
- N. Li, L. Zhang, Y. Chen, M. Fang, J. Zhang and H. Wang, *Adv. Funct. Mater.*, 2012, 22, 835-841.
- H. N. Kim, T. W. Kim, I. Y. Kim and S. J. Hwang, *Adv. Funct. Mater.*, 2011, 21, 3111-3118.
- B. Zhao, L. Lin and D. He, *J. Mater. Chem. A*, 2013, 1, 1659-1668.
- X. M. Sun and Y. D. Li, *Chem.-Eur. J.*, 2003, 9, 2229-2238.
- W. Liu, T. Wang, A. G. L. Borthwick, Y. Wang, X. Yin, X. Li and J. Ni, *Sci. Total. Environ.*, 2013, 456, 171-180.
- L. Xiong, C. Chen, Q. Chen and J. Ni, *J. Hazard. Mater.*, 2011, 189, 741-748.
- N. Li, L. Zhang, Y. Chen, Y. Tian and H. Wang, *J. Hazard. Mater.*, 2011, 189, 265-272.
- G. Sheng, S. Yang, J. Sheng, D. Zhao and X. Wang, *Chem. Eng. J.*, 2011, 168, 178-182.
- D. Yang, Z. Zheng, H. Liu, H. Zhu, X. Ke, Y. Xu, D. Wu and Y. Sun, *J. Phys. Chem. C*, 2008, 112, 16275-16280.
- D. Yang, S. Sarina, H. Zhu, H. Liu, Z. Zheng, M. Xie, S. V. Smith and S. Komarneni, *Angew. Chem. Int. Ed.*, 2011, 50, 10594-10598.
- G. Sheng and B. Hu, *J. Radioanal. Nucl. Chem.*, 2013, 298, 455-464.
- L. Wang, W. Liu, T. Wang and J. Ni, *Chem. Eng. J.*, 2013, 225, 153-163.
- G. Niu, W. Liu, T. Wang and J. Ni, *J. Colloid Interface Sci.*, 2013, 401, 133-140.
- H. Y. Niu, J. M. Wang, Y. L. Shi, Y. Q. Cai and F. S. Wei, *Micropor. Mesopor. Mater.*, 2009, 122, 28-35.
- Y. Wang, W. Liu, T. Wang and J. Ni, *J. Colloid Interface Sci.*, 2015, 440, 253-262.
- E. D. Stein, Y. Cohen and A. M. Winer, *Crit. Rev. Env. Sci. Tec.*, 1996, 26, 1-43.
- M. M. Matlock, B. S. Howerton and D. A. Atwood, *J. Hazard. Mater.*, 2001, 84, 73-82.
- R. Yan, F. Yang, Y. Wu, Z. Hu, B. Nath, L. Yang and Y. Fang, *Bioresour. Technol.*, 2011, 102, 9927-9932.
- S. Vasudevan, J. Lakshmi and G. Sozhan, *Environ. Sci. Pollut. R.*, 2012, 19, 2734-2744.
- J. Barron-Zambrano, S. Laborie, P. H. Viers, M. Rakib and G. Durand, *Desalination*, 2002, 144, 201-206.
- V. Gomez-Serrano, A. Macias-Garcia, A. Espinosa-Mansilla and C. Valenzuela-Calahorra, *Water Res.*, 1998, 32, 1-4.
- Y. Gong, Y. Liu, Z. Xiong and D. Zhao, *Environ. Sci. Technol.*, 2014, 48, 3986-3994.
- Q. R. Wang, D. Kim, D. D. Dionysiou, G. A. Sorial and D. Timberlake, *Environ. Pollut.*, 2004, 131, 323-336.
- C. Jeon and K. H. Park, *Water Res.*, 2005, 39, 3938-3944.
- W. Liu, W. Sun, Y. Han, M. Ahmad and J. Ni, *Colloids Surf. A*, 2014, 452, 138-147.
- T. Wang, W. Liu, N. Xu and J. Ni, *J. Hazard. Mater.*, 2013, 250, 379-386.

32. S. Brunauer, L. S. Deming, W. E. Deming and E. Teller, *J. Am. Chem. Soc.*, 1940, 62, 1723-1732.
33. J. Yu, J. C. Yu, M. K. P. Leung, W. Ho, B. Cheng, X. Zhao and J. Zhao, *J. Catal.*, 2003, 217, 69-78.
34. A. Turki, H. Kochkar, C. Guillard, G. Berhault and A. Ghorbel, *Appl. Catal. B-Environ.*, 2013, 138-139, 401-415.
35. S. Zhang, W. Xu, M. Zeng, J. Li, J. Li, J. Xu and X. Wang, *J. Mater.Chem. A*, 2013, 1, 11691-11697.
36. Y. S. Ho and G. McKay, *Chem. Eng. J.*, 1998, 70, 115-124.
37. Y. S. Ho and G. McKay, *Process Biochem.*, 1999, 34, 451-465.
38. I. Langmuir, *J. Am. Chem. Soc.*, 1918, 40, 1361-1403.
39. F. H. Z. *Phys. Chem.*, 1906, 57, 385-470.
40. K. Kadirvelu, M. Kavipriya, C. Karthika, N. Vennilamani and S. Pattabhi, *Carbon*, 2004, 42, 745-752.
41. M. J. Shadbad, A. Mohebbi and A. Soltani, *Korean J. Chem. Eng.*, 2011, 28, 1029-1034.
42. D. Perez-Quintanilla, I. del Hierro, M. Fajardo and I. Sierra, *J. Hazard. Mater.*, 2006, 134, 245-256.
43. S. K. Das, A. R. Das and A. K. Guha, *Environ. Sci. Technol.*, 2007, 41, 8281-8287.
44. S. Chiarle, M. Ratto and M. Rovatti, *Water Res.*, 2000, 34, 2971-2978.
45. W. Liu, P. Zhang, A. G. L. Borthwick, H. Chen and J. Ni, *J. Colloid Interface Sci.*, 2014, 423, 67-75.
46. R. G. Pearson, *J. Chem. Edu.*, 1968, 45, 581-&.
47. R. G. Pearson, *J. Chem. Edu.*, 1968, 45, 643-&.
48. R. G. Pearson, *Inorg. Chem.*, 1988, 27, 734-740.
49. B. J. *Chichester: Ellis Horwood*, 1978.
50. V. Stengl, S. Bakardjieva, J. Subrt, E. Vecernikova, L. Szatmary, M. Klementova and V. Balek, *Appl. Catal. B-Environ*, 2006, 63, 20-30.
51. K. Teshima, K. Yubuta, T. Shimodaira, T. Suzuki, M. Endo, T. Shishido and S. Oishi, *Cryst. Growth Des.*, 2008, 8, 465-469.
52. C. K. Lee, C. C. Wang, M. D. Lyu, L. C. Juang, S. S. Liu and S. H. Hung, *J. Colloid Interface Sci.*, 2007, 316, 562-569.
53. T. Wang, W. Liu, L. Xiong, N. Xu and J. Ni, *Chem. Eng. J.*, 2013, 215, 366-374.
54. H. Chen, X. Wang, J. Li and X. Wang, *Journal of Materials Chemistry A*, 2015, 3, 6073-6081.
55. H. Chen, J. Li, X. Wu and X. Wang, *Ind. Eng. Chem. Res.*, 2014, 53, 16051-16060.
56. C. Shan, Z. Ma, M. Tong and J. Ni, *Water Res.*, 2015, 69, 252-260.
57. R. Z. Ma, K. Fukuda, T. Sasaki, M. Osada and Y. Bando, *J. Phys. Chem. B*, 2005, 109, 6210-6214.
58. H. Liu, D. Yang, Z. Zheng, X. Ke, E. Waclawik, H. Zhu and R. L. Frost, *J. Raman Spectrosc.*, 2010, 41, 1331-1337.
59. W. Liu, J. Ni and X. Yin, *Water Res.*, 2014, 53, 12-25.
60. D. V. Bavykin, J. M. Friedrich, A. A. Lapkin and F. C. Walsh, *Chem. Mater.*, 2006, 18, 1124-1129.

Table of Contents



Hg(II) is trapped into titanate lattice with a phase transition from tri-titanate to hexa-titanate after adsorption